Hindawi
Mathematical Problems in Engineering
Volume 2018, Article ID 1359461, 15 pages
https://doi.org/10.1155/2018/1359461

Research Article

Design and Characteristics Analysis of a Nonlinear Isolator Using a Curved-Mount-Spring-Roller Mechanism as Negative Stiffness Element

Han Junshu, Meng Lingshuai, and Sun Jinggong

Institute of Medical Equipment, Academy of Military Medical Science, Tianjin 300161, China

Correspondence should be addressed to Sun Jinggong; sunjg@vip.sina.com

Received 29 January 2018; Accepted 15 April 2018; Published 6 June 2018

Academic Editor: Zhi-ke Peng

The characteristics of a passive nonlinear isolator are developed by combining a curved-mount-spring-roller mechanism as a negative stiffness corrector in parallel with a vertical linear spring. The static characteristics of the isolator are presented, and the configurative parameters are optimized to achieve a wider displacement range at the equilibrium position where the isolator has a low stiffness and the stiffness changes slightly. The restoring force of the isolator is approximated using a Taylor expansion to a cubic stiffness. Considering the overload and underload conditions, a dynamic equation is established as a Helmholtz-Duffing equation, and the resonance response of the nonlinear system is determined by employing the harmonic balance method (HBM). The frequency response curves (FRCs) are obtained for displacement excitations. The absolute displacement and acceleration transmissibility are defined and investigated to evaluate the performance of the nonlinear isolator, and they are compared with an equivalent linear isolator that can support the same mass with the same static deflection as the proposed isolator. The effects of the amplitude of the excitation, the offset displacement, and the damping ratio on the dynamic characteristics and the transmissibility performance are considered, and experiments are carried out to verify the above analysis. The results show that the overload and underload system can outperform the counterparts with the linear stiffness, softening stiffness, softening-hardening stiffness, and hardening stiffness with the magnitude of the excitation amplitude, and that its isolation performance is generally better than that of a linear system. The transmissibility, response, and resonance frequency of the system are affected by the excitation amplitude, offset displacement, cubic stiffness, and damping ratio. To obtain a better isolation performance, an appropriate mass, not-too-large amplitude, and larger damper are necessary for the proposed isolator.

1. Introduction

The purpose of vibration isolation is to avoid or reduce the undesirable effects of vibration with the aid of a device that isolates the vibration sources. Currently, passive vibration isolation and control is the most prevalent vibration-isolating approach. The theory for both passive linear and nonlinear vibration isolation has been fully studied [1–3]. A linear vibration isolator is the simplest and most effective passive vibration isolator, but such an isolator has a fixed stiffness and can only isolate a vibration that is $\sqrt{2}$ times greater than the inherent frequency of the isolator, with a poor capability to isolate low-frequency vibrations [4]. However, a nonlinear vibration isolator can obtain a lower dynamic stiffness and a higher static-carrying capacity, leading to an outstanding low-frequency vibration isolation performance [5]. Therefore, theories and applications of nonlinear vibration isolators have gained popularity among scholars and have become a hot topic in research.

Nonlinear vibration isolators may be realized with special structures or devices. For example, Virgin and Davis created a nonlinear vibration isolator with curved beam structures [6]. Zhang et al. [7] used a beam under axial force at its two ends to get the same kind of stiffness. Molyneux [8] developed a structure composed of two inclined springs to get very low stiffness. According to the most commonly available approach, quasi-zero stiffness is realized through parallel positive and negative stiffness. The positive stiffness is generally generated by a compression spring, while the negative stiffness is realized by a variety of means, such as springs,

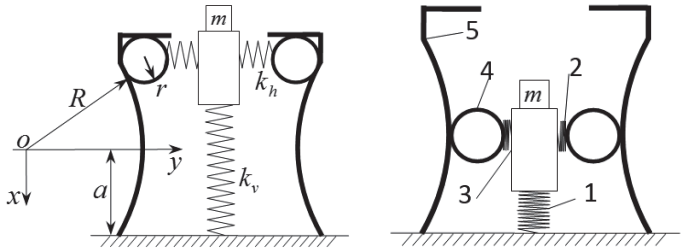

(a) Initial position (b) Equilibrium position

Figure 1: Prototype model of the proposed QZS isolator.

magnets, electromagnetism, and buckle beams [9]. Depending on differences in the size of the target position space, the bearing capacity, and the frequency band that must be isolated, different structural forms are adopted to gain negative stiffness. Carrella et al. studied an isolating system with a three-spring structure and performed an analysis of the static and dynamic characteristics and an optimization of the system [10, 11]. Kovacic made some improvements to a three-spring structure by replacing the oblique spring with two nonlinear springs, thereby obtaining a system with lower stiffness and a wider displacement range near the equilibrium position [12, 13]. Thanh applied a connecting rod-spring mechanism as a negative stiffness element to isolate vibrations on vehicle seats and experimentally verified the excellent performance of the mechanism [14, 15]. Alabuzhev et al. [16, 17] investigated the effect of a stiffness corrector that acts as a negative stiffness structure to improve the isolation performance and summarized many prototypes characterized by quasi-zero stiffness. Platus [18, 19] exploited two bars hinged at the center and loaded in compression to get negative stiffness. Yang studied the kinetics and power spectrum characteristics of a negative stiffness mechanism composed of two mutually articulating bars that articulated under an axial load [19, 20]. Guangjun et al. established a static model using a thin-walled beam structure as the negative stiffness element and conducted an experimental study [21]. Xingtian et al. created a quasi-zero-stiffness vibration isolator using a symmetric skewed Euler beam as the negative stiffness element and theoretically studied the effects of the excitation amplitude, damping ratio, and other such parameters on the frequency response characteristics and vibration isolation performance of the system [22–24]. Zhenhua studied a spherical roller-based nonlinear suspension and analyzed the corresponding frequency component of the system under harmonic excitation based on a Fourier transform [25]. Lingshuai designed a novel quasi-zero-stiffness isolator by combining a disk spring and a linear coil spring and analyzed the static and dynamic characteristics of the isolator [26]. Xudong studied a quasi-zero-stiffness isolator, which consisted of air springs, by analyzing both the static and dynamic characteristics of the quasi-zero-stiffness isolator and applying the system to the isolation of vibrations in an off-road ambulance stretcher [27].

For the on-board precision instruments on the off-road vehicles, the low-frequency vibration of 0.5–70 Hz is the major damage frequency. To improve the vibration isolation for the on-board precision instruments on the off-road vehicles, a low-frequency isolator is proposed. In this paper, a nonlinear isolator is developed by combining a curved-mount-spring-roller mechanism with a vertical linear spring as shown in Figure 1. The mass is supported by a vertical linear spring with a static deflection. At this position, the curved-mount-spring-roller mechanism is arranged onto the mass horizontally to give no vertical restoring force, while the mechanism can adjust the stiffness of the linear spring by deflecting in the horizontal direction. The proposed isolator composed of three linear springs is simple and convenient to use, occupying small space; it can offer greater support capacity and greater displacement range. Therefore, it is suitable for being used for the occasion with space limitation for isolators, and especially a limitation in the vertical direction. The supported load can be adjusted according to needs. The aims of this study are to design a nonlinear isolator and its configurative parameters, investigate its static and dynamic characteristics and the effects of overload or underload on the isolation performance of the proposed isolator, and build an experimental apparatus to verify the isolation performance of the overloaded isolator.

2. Static Characteristics of the Nonlinear Isolator

2.1. Static Model of the Isolator. A negative stiffness mechanism is unstable, so it cannot work as an isolator alone. However, it can be combined with a positive stiffness element, i.e., a linear spring, to get an isolator that cancels the positive stiffness. As shown in Figure 1, the proposed curved-mount-spring-roller isolator is composed of a vertical spring (1), two horizontal springs (2), a holder (3), a roller (4), and a curved mount (5). The curved mount is connected to a base such as a carriage floor, and the holder supports the mass moving up and down with the vertical spring. The roller can roll up and down along the track on the curved mount. When the mechanism is at the equilibrium position presented in Figure 1(b), the rollers contact the highest point on the curved surface of the curved mount. This is the working position of the mechanism. The configurative parameters are the vertical spring stiffness k_v, stiffness of the horizontal springs k_h, radius of the roller r, and the radius of the curved mount R. The chord length of the curved surface is $2a$.

It is assumed that both the vertical spring and the horizontal spring are in a relaxed condition at the initial state $x = -h$, as shown in Figure 1(a). With the mechanism moving down from the initial state, the horizontal springs are compressed. They can provide a restoring force in the vertical direction, which can cancel the restoring force provided by the vertical one. When the mechanism reaches the equilibrium position $x = 0$, it just can cancel all the restoring force of the vertical spring. Based on the analysis given above, the nondimensional force-displacement relationship of the isolator can be obtained from

$$F = x\left(k_v - 2k_h\right) - h + u_v + \frac{2k_h x\left(\sqrt{R^2 - a^2} + r - u_h\right)}{\sqrt{(R+r)^2 - x^2}} \quad (1)$$

Define the nondimensional parameters:

$$\begin{aligned} \alpha &= \frac{r}{R}, \\ \beta &= \frac{a}{R}, \\ \widehat{u}_h &= \frac{u_h}{R}, \\ \widehat{F} &= \frac{F}{k_v \cdot R}, \\ \widehat{u}_v &= \frac{u_v}{R}, \\ \lambda &= \frac{k_h}{k_v}, \\ \widehat{h} &= \frac{h}{R}, \\ \widehat{x} &= \frac{x}{R} \end{aligned} \quad (2)$$

The restoring force can be written in the nondimensional form as follows:

$$\widehat{F} = \widehat{x}\,(1 - 2\lambda) - \widehat{h} + \widehat{u}_v + \frac{2\lambda\widehat{x}\left(\sqrt{1-\beta^2} + \alpha - \widehat{u}_h\right)}{\sqrt{(1+\alpha)^2 - \widehat{x}^2}} \quad (3)$$

Differentiating (3) with respect to the nondimensional displacement $\widehat{x}$, the nondimensional stiffness of the isolator can be obtained. Both the nondimensional force and stiffness of the isolator are a function of the nondimensional displacement.

$$\widehat{k} = 1 - 2\lambda + \frac{2\lambda\,(1+\alpha)^2\left(\sqrt{1-\beta^2} + \alpha - \widehat{u}_h\right)}{\sqrt{\left[(1+\alpha)^2 - \widehat{x}^2\right]^3}} \quad (4)$$

By differentiating (4) with respect to the nondimensional displacement, the following can be yielded:

$$\widehat{k}' = \left(\sqrt{1-\beta^2} + \alpha - \widehat{u}_h\right) \cdot \frac{6\lambda\,(1+\alpha)^2 \cdot \widehat{x}}{\sqrt{\left[(1+\alpha)^2 - \widehat{x}^2\right]^5}} \quad (5)$$

For $\widehat{x} = 0$, it can be derived from (5) that $\widehat{k}' = 0$. Therefore, the nondimensional stiffness of the nonlinear isolator has a minimum at the equilibrium position $\widehat{x}_e = 0$ and is given by

$$\widehat{k}_{\min} = 1 - 2\lambda + \frac{2\lambda\left(\sqrt{1-\beta^2} + \alpha - \widehat{u}_h\right)}{1+\alpha} \quad (6)$$

The minimum stiffness at the static equilibrium position is set to zero. Then, the stiffness ratio that yields the quasi-zero stiffness is as follows:

$$\lambda = \frac{1+\alpha}{2\left(1 - \sqrt{1-\beta^2} + \widehat{u}_h\right)} \quad (7)$$

Eq. (7) is the zero-stiffness condition of the isolator. When λ, α, β, and $\widehat{u}_h$ satisfy (7), the isolator has a zero-stiffness point. Substituting (7) into (4), then the stiffness expression can be obtained as (8), where it can be seen that the nondimensional stiffness is a function of the nondimensional displacement which is affected by the configurative parameters of the mechanism and its trough is zero:

$$\begin{aligned} \widehat{k} = 1 &- \frac{1+\alpha}{1 - \sqrt{1-\beta^2} + \widehat{u}_h} + \frac{1+\alpha}{1 - \sqrt{1-\beta^2} + \widehat{u}_h} \\ &\cdot \frac{(1+\alpha)^2\left(\sqrt{1-\beta^2} + \alpha - \widehat{u}_h\right)}{\sqrt{\left[(1+\alpha)^2 - \widehat{x}^2\right]^3}} \end{aligned} \quad (8)$$

2.2. Optimization of the Isolator. According to the above analysis, it is possible for the mechanism to have zero stiffness with appropriate matching parameters. Except for a zero-stiffness property, it is desirable for the isolator to have low nondimensional stiffness in a wide range of nondimensional displacements $\widehat{d}$ from the static equilibrium position.

Substituting $\widehat{x} = \widehat{x}_e \pm \widehat{d} = \pm\widehat{d}$ into (4), the relationship between the nondimensional displacement $\widehat{d}$ and the configurative parameters is obtained as

$$\widehat{d} = \sqrt{(1+\alpha)^2 - \left[\frac{2\lambda\,(1+\alpha)^2\left(\sqrt{1-\beta^2} + \alpha - u_h\right)}{\widehat{k} - 1 + 2\lambda}\right]^{2/3}} \quad (9)$$

It can be seen that the nondimensional displacement is determined by the configurative parameters α, β, $\widehat{u}_h$, and the stiffness λ. They are chosen from the set $0.1 < \alpha \le 0.5$, $0.5 < \beta \le 1$, $0 \le \widehat{u}_h \le 1$, and $0.1 < \lambda \le 5$ according to the practical engineering conditions and the special requirements of the mechanism in the practical vehicle application. Note that the stiffness ratio calculated using (7) should be positive, and the stiffness also should not be negative. The optimization criteria include the condition that the largest displacement is achieved when the stiffness of the isolator is equal to that

Table 1: Optimal and other configurative parameters of the isolator.

Groups	Parameter value			
	α	β	λ	$\widehat{u}_h$
1	0.3	0.4777	2.022	0.2
2	0.28	0.69	1.9839	0.0464
3	0.28	0.3097	4.2905	0.1
4	0.26	0.276	1.6033	0.3541

of the linear spring, i.e., $\lambda = 1$, and the requirement that the nondimensional stiffness changes slightly with the tolerance of $\Delta\widehat{k} = 0.25$ for $\Delta\widehat{x} = 0.01$ in the region around the equilibrium position. Then, the optimization mathematical model can be obtained as

$$\begin{aligned} \max \quad & f(X) = f(x_1, x_2, \ldots, x_n) \\ \text{s.t.} \quad & G_j(X) = G_j(x_1, x_2, \ldots, x_n) \quad (j = 1, 2, \ldots, q) \\ & 0 \le F_i(x_1, x_2, \ldots, x_n) \le 1 \quad (i = 1, 2, \ldots, m) \\ & 0 < F_i(x_1, x_2, \ldots, x_n) < 0.868 \quad (i = 1, 2, \ldots, m) \\ & h_k(X) = h_k(x_1, x_2, \ldots, x_n) = 0.25 \quad (k = 1, 2, \ldots, p), \end{aligned} \tag{10}$$

where $n = 4$, $x_1 = \alpha$, $x_2 = \beta$, $x_3 = \lambda$, $x_4 = u_h$, $q = 1$, $m = 15$, and $p = 10$.

Based on the calculation through a genetic algorithm, the optimization results are $\alpha = 0.3$, $\beta = 0.4777$, and $\widehat{u}_h = 0.2$, and the nondimensional displacement is $\widehat{d} = 0.52$. We get the optimal parameters (Group 1) and other parameters satisfying the optimization criteria listed in Table 1 and plot the stiffness-displacement curves in Figure 2. It is obvious that the optimized isolator has a very small stiffness in the region around the equilibrium position, and a larger displacement from the static equilibrium position with a smaller stiffness.

2.3. Approximation of the Restoring Force. To simplify the expression of the restoring force, which is very complicated, (1) can be expanded to a third-order Taylor series at the zero-stiffness position $\widehat{x} = 0$ by neglecting the higher-order terms. The approximate restoring force is given by

$$\widehat{F}_{\text{app}}(\widehat{x}) \approx \chi + k_3 \widehat{x}^3, \tag{11}$$

where $\chi = -\widehat{x}_0 + \widehat{u}_v$, $k_3 = \lambda((\sqrt{1-\beta^2} + \alpha - \widehat{u}_h)/(1+\alpha)^3)$, where χ and the cubic stiffness k_3 are the parameters defined for simplicity. The exact restoring force expressed by (3) and the approximate restoring force expressed by (4) are plotted in Figure 3 for the optimal parameters, that is, Group 1 in Table 1. Note that the error of the approximation depends on the nondimensional displacement and less than 10% for the region $|\widehat{x}| \le 0.6$.

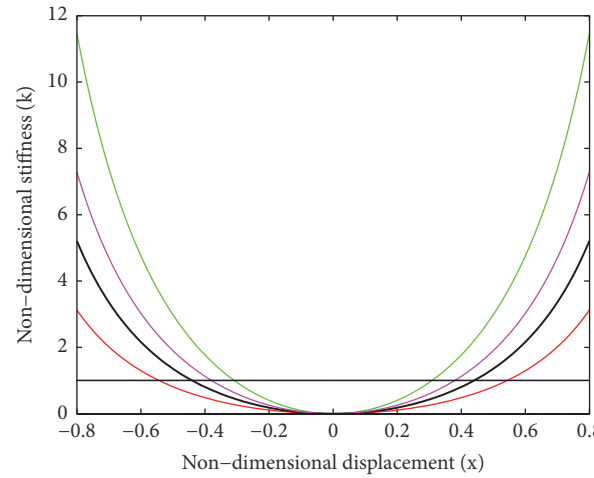

Figure 2: Nondimensional stiffness characteristics of the isolator for different configurative parameters.

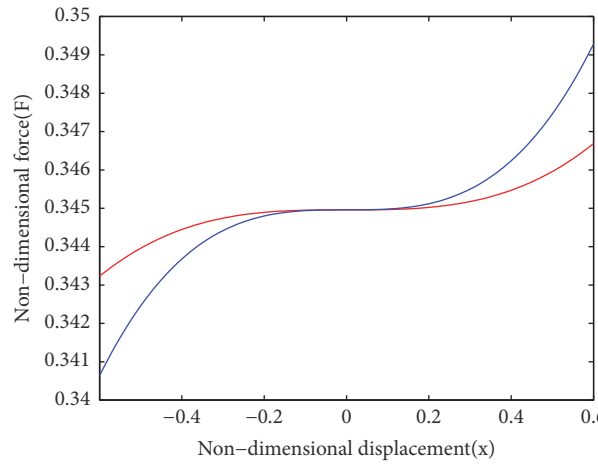

Figure 3: Nondimensional force-displacement of the isolator for optimal parameters. "Red line" is the exact restoring force. "Blue line" is the approximate restoring force.

3. Dynamic Characteristics of the Nonlinear Isolator

3.1. Setting Up the Differential Equation of the Motion and the Approximate Solution. In the ideal condition loaded with an appropriate mass called rated mass m_0, the isolator will be balanced at the equilibrium position $\widehat{x} = 0$. For this condition, the negative stiffness can completely cancel the positive stiffness at this point, which means that the stiffness at this point is zero, as shown in Figure 4(a). The mass is

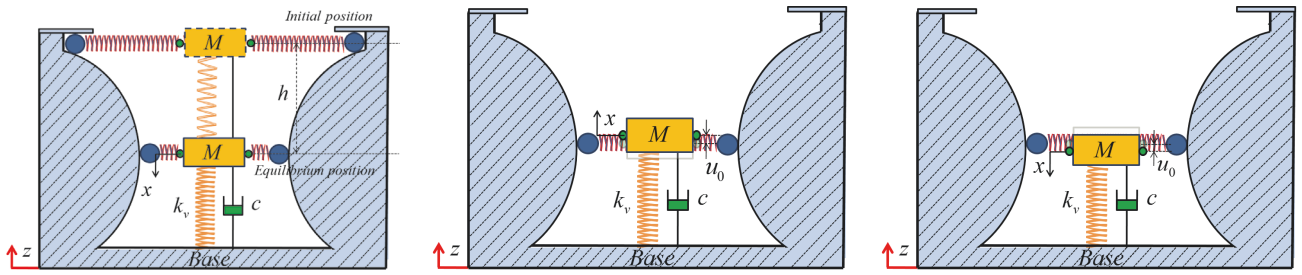

FIGURE 4: Schematic representation of the proposed isolator. (a) Ideal state for rated load, (b) isolator in overload state, and (c) isolator in underload state.

supported by the vertical spring, with the restoring force provided by the horizontal springs at zero at this point. If the isolated mass is not just the rated mass, i.e., $m \neq m_0$, the system will not balance at the zero-stiffness point; rather, it will be balanced at $\hat{x} = +\hat{u}_0$ for $m > m_0$. This is called the "overload state"; by contrast, $\hat{x} = -\hat{u}_0$ for $m < m_0$ is called the "underload state", and $\hat{u}_0$ is called the offset displacement illustrated in Figures 4(b) and 4(c). In this static state, the system is found to satisfy the following equilibrium equation:

$$\text{Overload state:} \quad k_v \cdot R \cdot \hat{f}(\hat{x}) = k_v \cdot R \cdot \left(\chi + \gamma \hat{u}_0^{\,3}\right) = mg \tag{12a}$$

$$\text{Underload state:} \quad k_v \cdot R \cdot \hat{f}(\hat{x}) = k_v \cdot R \cdot \left(\chi - \gamma \hat{u}_0^{\,3}\right) = mg \tag{12b}$$

In practical operation, mass changes frequently occur in practical situations, and it is difficult to ensure that the system is balanced at $\hat{x} = 0$. Thus, it is significant to consider the isolator under an overload or underload condition. When balanced at $\hat{x} = u_0$ or $\hat{x} = -u_0$, the stiffness of the isolator at the equilibrium position is never the minimum stiffness according to Figure 5. It can be found that the stiffness of the isolator in an overload state is lower than that of the linear isolator but larger than that of the ideal state of the isolator. In the figure, "o" indicates an overload system, and "$*$" indicates an underload system. Thus, the isolation performance of the isolator under these conditions should be different than when the isolator is loaded at a rated mass.

Assuming that the isolator is balanced at the new static equilibrium point and is exposed to a base displacement excitation $z = Z_0 \cos(\omega t)$, where Z_0 is the amplitude and ω is the excitation frequency, and applying Newton's second law of motion, the differential motion equation of the isolated mass can be determined as

$$m\ddot{u} + c\dot{u} + F(u \pm u_0) - mg = -m\ddot{z}, \tag{13}$$

where $u = x - z$ is the relative displacement between the isolated mass and the base and $F(u \pm u_0)$ is the restoring force of the system. By combining (12a), (12b), and (13), the following nondimensional parameters are obtained:

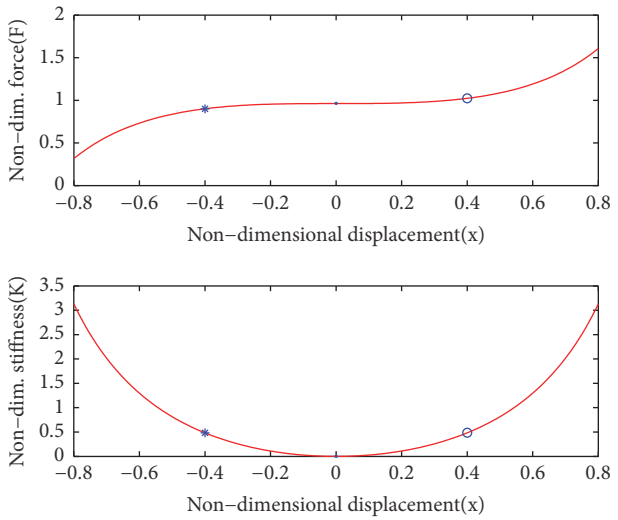

FIGURE 5: Nondimensional stiffness-displacement curve of the system under rated-load, overload, and underload conditions: (•) equilibrium point at the rated state, (o) equilibrium point in overload state, and (∗) equilibrium point in underload state.

$$\begin{aligned} \tau &= \omega_n t, \\ \Omega &= \frac{\omega}{\omega_n}, \\ \omega_n &= \sqrt{\frac{k_v}{m}}, \\ \hat{u} &= \frac{u}{R}, \\ \xi &= \frac{c}{2m\omega_n}, \\ \hat{F} &= \frac{F}{k_v R}, \\ \hat{Z}_0 &= \frac{Z_0}{R}, \end{aligned} \tag{14}$$

where $\omega_n = \sqrt{k_v/m}$ is the undamped natural frequency of the system without a negative stiffness mechanism.

In terms of these nondimensional parameters, (10) can be rewritten as

$$\hat{u}'' + 2\xi\hat{u}' + k_3\left(\hat{u} \pm \hat{u}_0\right)^3 = \Omega^2\widehat{Z}_0\cos\left(\Omega\tau\right), \tag{15}$$

where a prime denotes the nondimensional time (τ) derivative, and the unknown phase difference between the excitation and response is added to the excitation.

By rewriting (15), the nondimensional approximate dynamic equation that expresses the steady-state vibration of the isolated mass around the equilibrium position can be obtained:

$$\hat{u}'' + 2\xi\hat{u}' + n_1\hat{u} \pm n_2\hat{u}^2 + k_3\hat{u}^3 = \Omega^2\widehat{Z}_0\cos\left(\Omega\tau\right), \tag{16}$$

where $n_1 = 3k_3{u_0}^2$, $n_2 = 3k_3u_0$, and +/− denotes "overload" and "underload", respectively. Eq. (16) is the well-known Helmholtz-Duffing equation, which can be recast in the form of a Duffing oscillator under asymmetric excitation.

By setting and substituting $\hat{v} = \hat{u} \pm \hat{u}_0$ into (16), the nondimensional approximate steady-state dynamic equation is

$$\hat{v}'' + 2\xi\hat{v}' + k_3\hat{v}^3 = \pm k_0 + \Omega^2\widehat{Z}_0\cos\left(\Omega\tau\right), \tag{17}$$

where $k_0 = k_3{\hat{u}_0}^3$. In order to find the steady-state response of the system, the Harmonic Balance Method is a useful approach [28]. Here, the approximate steady-state solution of (17) can be assumed to be

$$\hat{v} = A_0 + A_1\cos\left(\Omega\tau + \varphi\right), \tag{18}$$

where A_0 and A_1 represent the amplitude of the constant and the harmonic terms for the steady-state response, respectively. Substituting (18) into (17) and neglecting the higher harmonic terms, the following can be obtained:

$$\begin{aligned}&\left(-\Omega^2A_1 + k_1A_1 + 3k_3{A_0}^2A_1 + \frac{3}{4}k_3{A_1}^3\right)\cos\left(\Omega\tau\right)\\ &\quad - 2\xi A_0\Omega\sin\left(\Omega\tau\right) + k_1A_0 + k_3{A_0}^3 + \frac{3}{2}k_3A_0{A_1}^2\\ &\quad = \pm k_0 + \widehat{Z}_0\Omega^2\cos\left(\Omega\tau\right)\cos\varphi + \widehat{Z}_0\Omega^2\sin\left(\Omega\tau\right)\sin\varphi\end{aligned} \tag{19}$$

By equating the coefficients of the same cosines and sines from both sides of (19), the steady-state condition expressed by the following algebraic equations in terms of a bias term A_0, the amplitude of the harmonic term A_1, and the phase φ can be determined:

$$k_3{A_0}^3 + \frac{3k_3A_0{A_1}^2}{2} = \pm k_0 \tag{20a}$$

$$-A_1\Omega^2 + 3k_3{A_0}^2A_1 + \frac{3}{4}k_3{A_1}^3 = \Omega^2\widehat{Z}_0\cos\varphi \tag{20b}$$

$$-2\xi A_1\Omega = \Omega^2\widehat{Z}_0\sin\varphi \tag{20c}$$

Combining (20a), squaring, and adding (20b) and (20c) lead to a frequency-amplitude relationship as follows:

$$\begin{aligned}&25\gamma^3{A_0}^9 - 20{k_3}^2\Omega^2{A_0}^7 - 15{k_3}^2k_0{A_0}^6\\ &\quad + 4k_3\Omega^2\left(\Omega^2 + 4\xi^2\right){A_0}^5 + 16k_3k_0\Omega^2{A_0}^4\\ &\quad + 3k_3\left(2{\widehat{Z}_0}^2\Omega^4 - 3{k_0}^2\right){A_0}^3\\ &\quad - 4k_0\Omega^2\left(\Omega^2 + 4\xi^2\right){A_0}^2 + 4{k_0}^2\Omega^2A_0 - {k_0}^3 = 0\end{aligned} \tag{21a}$$

$$\begin{aligned}&25{k_3}^3{A_0}^9 - 20{k_3}^2\Omega^2{A_0}^7 + 15{k_3}^2k_0{A_0}^6\\ &\quad + 4k_3\Omega^2\left(\Omega^2 + 4\xi^2\right){A_0}^5 - 16k_3k_0\Omega^2{A_0}^4\\ &\quad + 3k_3\left(2{\widehat{Z}_0}^2\Omega^4 - 3{k_0}^2\right){A_0}^3\\ &\quad + 4k_0\Omega^2\left(\Omega^2 + 4\xi^2\right){A_0}^2 + 4{k_0}^2\Omega^2A_0 + {k_0}^3 = 0\end{aligned} \tag{21b}$$

Eqs. (21a) and (21b) are the implicit equations for the amplitude of the bias term A_0. They are valid for the equilibrium points at $u = +u_0$ and $u = -u_0$, respectively, corresponding to the "overload" and "underload" states.

By solving (21a) and (21b) and combining the result with (20a), the response of the mass under base excitation can be obtained for the determined system parameters. Eqs. (21a) and (21b) can be taken as a quadratic polynomial about Ω^2. Then, the implicit equation for the peak amplitudes A^o_{0p} and A^u_{0p} of the bias term and the corresponding frequency Ω^o_{0p} (Ω^u_{0p}) can be derived as follows in (22a) and (22b) for "overload" and (23a) and (23b) for "underload":

$$\begin{aligned}&\left(-75{k_3}^4{\widehat{Z}_0}^2 - 80{k_3}^3\xi^2\right)A^{d9}_{0p} + 32{k_3}^2\xi^4A^{d7}_{0p}\\ &\quad + \left(45{k_3}^3k_0{\widehat{Z}_0}^2 + 144{k_3}^2k_0\xi^2\right)A^{d6}_{0p} - 64k_3k_0\xi^4A^{d4}_{0p}\\ &\quad + \left(27{k_3}^2{k_0}^2{\widehat{Z}_0}^2 - 48k_3{k_0}^2\xi^2\right)A^{d3}_{0p} + 32{k_0}^2\xi^4A^{d}_{0p}\\ &\quad + \left(3k_3{k_0}^3{\widehat{Z}_0}^2 - 16{k_0}^3\xi^2\right) = 0\end{aligned} \tag{22a}$$

$$\Omega^o_{0p} = \sqrt{\frac{5{k_3}^2{A^o_{0d}}^6 - 4k_3\xi^2{A^o_{0d}}^4 - 4k_3k_0{A^o_{0d}}^3 + 4k_0\xi^2A^o_{0d} - {k_0}^2}{2k_3{A^o_{0d}}^4 + 3k_3{\widehat{Z}_0}^2{A^o_{0d}}^2 - 2k_0A^o_{0d}}} \tag{22b}$$

$$\begin{aligned}&\left(-75{k_3}^4{\widehat{Z}_0}^2 - 80{k_3}^3\xi^2\right){A^u_{0d}}^9 + 32{k_3}^2\xi^4{A^u_{0d}}^7\\ &\quad - \left(45{k_3}^3k_0{\widehat{Z}_0}^2 + 144{k_3}^2k_0\xi^2\right){A^u_{0d}}^6 + 64k_3k_0\xi^4{A^u_{0d}}^4\\ &\quad + \left(27{k_3}^2{k_0}^2{\widehat{Z}_0}^2 - 48k_3{k_0}^2\xi^2\right){A^u_{0d}}^3 + 32{k_0}^2\xi^4A^u_{0d}\\ &\quad - 3k_3{k_0}^3{\widehat{Z}_0}^2 + 16{k_0}^3\xi^2 = 0\end{aligned} \tag{23a}$$

$${\Omega_{0_p}}^u = \sqrt{\frac{5{k_3}^2{A_{0_p}}^6 - 4k_3\xi^2{A^u_{0p}}^4 + 4k_3k_0{A^u_{0p}}^3 - 4k_0\xi^2A^u_{0p} - {k_0}^2}{2k_3{A^u_{0p}}^4 + 3k_3{\widehat{Z}_0}^2{A^u_{0p}}^2 + 2k_0A^u_{0p}}} \tag{23b}$$

By combining (22a)-(22b) and (23a)-(23b) with (20a), the amplitude of the harmonic term A_1 and its peak amplitudes A_{1p}^o and A_{1p}^u can be derived. The frequency response curves (FRCs) of the overload and underload system are determined by (21a) and (21b).

As stated above, for the ideal isolator with an equilibrium position at $\widehat{u} = 0$, its steady-state solutions under displacement excitations can be derived by setting $\widehat{u}_0 = 0$ through the procedure above. And its nondimensional approximate steady-state dynamic equation for the displacement excitation is

$$\widehat{v}'' + 2\xi\widehat{v}' + k_3\widehat{v}^3 = Z_0\Omega^2\cos(\Omega\tau) \tag{24}$$

Then the amplitude frequency equation can be derived as below, and the peak amplitude A_{1p} of the response and the related frequency Ω_p can be achieved.

$$\frac{9}{16}{k_3}^2{A_1}^6 - \frac{3}{2}k_3\Omega^2{A_1}^4 + \Omega^2\left(\Omega^2 + 4\xi^2\right){A_1}^2 - \Omega^4{\widehat{Z}_0}^2 = 0 \tag{25a}$$

$$A_{1p} = \frac{8\xi^2}{\sqrt{48k_3\xi^2 - 9{k_3}^2{Z_0}^2}} \tag{25b}$$

$$\Omega_p = \xi^3\sqrt{\frac{24k_3{Z_0}^2 - 64\xi^2}{64\xi^6 - 60\xi^4{Z_0}^2 + 18{k_3}^2\xi^2{Z_0}^4 - 27{k_3}^3{Z_0}^6}} \tag{25c}$$

By removing the negative stiffness mechanism, the equivalent linear system corresponding to the ideal system can be acquired. Its dynamic equation and its amplitude of the steady-state response are as follows:

$$\widehat{v}'' + 2\xi\widehat{v}' + \widehat{v} = \widehat{Z}_0\Omega^2\cos(\Omega\tau) \tag{26a}$$

$$A = \frac{\widehat{Z}_0\Omega^2}{\sqrt{\left(1-\Omega^2\right)^2 + (2\xi\Omega)^2}} \tag{26b}$$

3.2. Effects of the Offset Displacement, Excitation Amplitude, Damping Ratio, and Cubic Stiffness on the Transmissibility. The optimal configurative parameters illuminated in Section 2.2 and the damping ratio $\xi = 0.03$ are used to conduct the following investigations. For the displacement excitations, the values of the offset displacement $\widehat{u}_0$, excitation amplitude $\widehat{Z}_0$, damping ratio ξ, and cubic stiffness k_3 are chosen to study their effects on the nonlinear isolator. The FRCs of the ideal system and the equivalent linear system are also illustrated for comparison. Three offset displacements, four excitation levels, four damping ratio values, and four cubic stiffness values are studied. The relative result curves are presented in Figures 6–8 with "red dashed line" denoting unstable solutions, "black solid line" denoting stable solutions, and "o" displaying the peak response.

For a system with a certain nonzero offset displacement as shown in Figures 4(b) and 4(c), under the displacement excitation, the bias and harmonic terms of the response both exist. With an increase in the excitation amplitude, the amplitude of the harmonic term A_1 increases, and it may appear unbounded. Obviously, the effect of the excitation amplitude on the bias term A_0 is only around the resonance frequency. In this region, a larger excitation amplitude leads to a smaller peak amplitude of the bias term. Far away from this region, the bias term A_0 changes a little and approaches the value of the offset displacement $\widehat{u}_0$. The resonance frequency of the system decreases at first, then increases later, and becomes larger as the excitation amplitude increases continuously. This is different in that both the amplitude of the response A_{1p} and resonance frequency Ω_p of the ideal isolator increase with an increasing excitation amplitude. In other words, for the ideal system, the stiffness characteristics exhibit linear stiffness when the excitation amplitude is small, and as the excitation amplitude increases, it exhibits the hardening stiffness feature.

However, for an overload or underload system, it might exhibit softening stiffness, softening-hardening stiffness, or hardening stiffness, which change along with the excitation amplitude. With an increase in the excitation amplitude, the number of steady-state solutions of the overload system increases. This number may be a maximum of five, three, or one, and multiple jumps occur. Kovacic et al. confirmed the same conclusion for a force excitation [12, 13]. It also can be seen that, for an overload or underload system, the harmonic term amplitudes A_1 of the response are the same, but the bias term amplitudes A_0 are symmetric about $A_0 = 0$, which is the static equilibrium position of the system loaded by the rated mass.

For the same displacement excitation, a decrease in the offset displacement $\widehat{u}_0$ results in a decrease in the bias term amplitude A_0, the harmonic term amplitudeA_1, and resonance frequency Ω_p. The bias term amplitude disappears when $\widehat{u}_0 = 0$. When the offset displacement is fixed, when the cubic stiffness increases, the bias term amplitude and the peak of A_0 decrease, but the harmonic term amplitude, the peak of A_1, and the corresponding resonance frequency for the peak increase instead. The number of steady-state solutions also increases. In addition, it can be found in Figure 7 that the effects of the cubic stiffness and offset displacement on an overload and underload system are the same, but the sign of the bias term is related to the state of overload or underload, and the response amplitude is related not to the offset direction but its magnitude.

The effects of the damping ratio on the FRCs are prominent around the resonance frequency. In this region, when the damping ratio increases, the harmonic term amplitude and the peak amplitude decrease, but the bias term amplitude and the peak amplitude increase. The resonance frequency for the peak amplitude increases first and then decreases later. When the damping ratio is under a certain value, the harmonic term amplitude appears as an unbounded value, and the bias term amplitude tends to zero. For the same damping ratio value, bias term, and harmonic term amplitude, their peak amplitude and corresponding resonance frequency increase as the offset displacement increases.

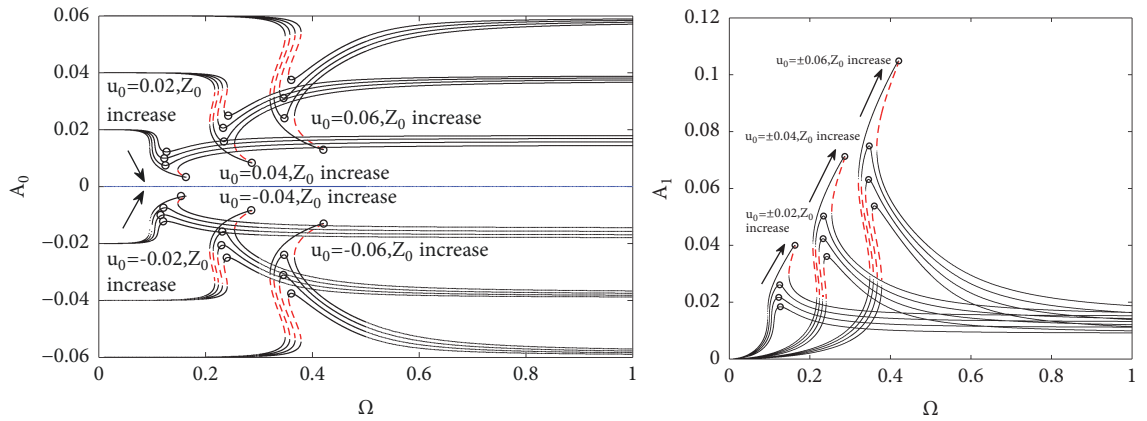

Figure 6: FRCs of overload and underload system with different offset displacements and excitation amplitudes for the displacement excitation.

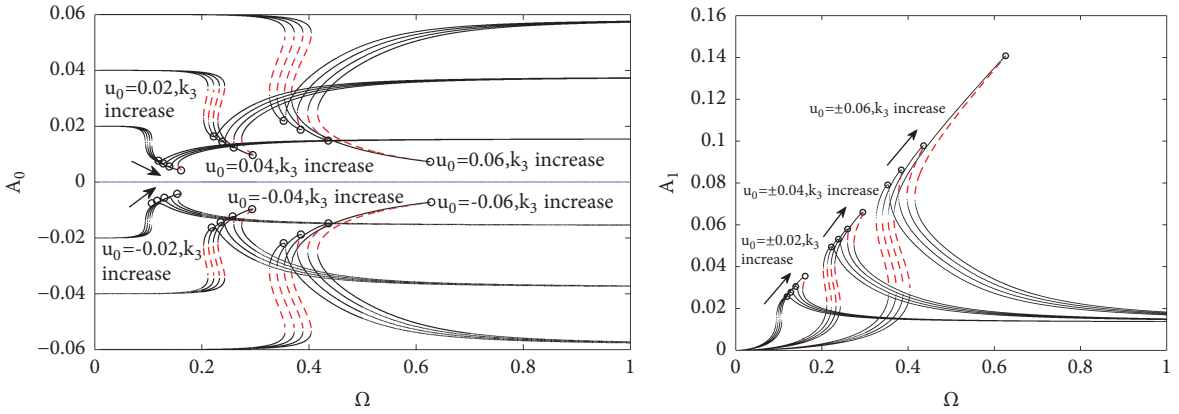

Figure 7: FRCs of overload and underload system with different offset displacements and cubic stiffness for the displacement excitation.

3.3. Effects of the Offset Displacement, Excitation Amplitude, and Damping Ratio on the Transmissibility. The absolute displacement transmissibility and the absolute acceleration transmissibility are the key indices for evaluating the performance of an isolator excited by the displacement excitation. From (17), the overloaded nonlinear isolator is a nonlinear isolator with asymmetric restoring force, and its steady-state response contains a constant term A_0. Thus, it is not sufficient to evaluate the isolation performance of this kind of isolators by using only one of the indexes. The absolute displacement transmissibility can account for the effect of the constant term on the isolation performance. In this section, the absolute displacement and acceleration transmissibility are defined and investigated to evaluate the isolation performance of overload and underload systems, and they are compared with those of an ideal system and the equivalent linear system.

3.3.1. Definition of the Transmissibility. The absolute displacement transmissibility is defined as the ratio between the amplitude of the absolute displacement of the mass and the excitation displacement. It is given by

$$T_D = \frac{\widehat{u}}{\widehat{z}}, \tag{27}$$

where $\widehat{u}$ represents the nondimensional absolute displacement of the mass and $\widehat{z}$ is the nondimensional excitation displacement. Under the displacement excitation, the nondimensional absolute displacement of the mass for an overload or underload system can be expressed by

$$\begin{aligned}\widehat{u} &= \widehat{v} \mp \widehat{u}_0 + \widehat{z} \\ &= A_0 \mp \widehat{u}_0 + A_1 \cos(\Omega\tau + \varphi) + \widehat{Z}_0 \cos(\Omega\tau)\end{aligned} \tag{28}$$

And then its absolute displacement transmissibility can be obtained by

$$\begin{aligned}T_{\text{disp}} &= \left|\frac{\widehat{u}}{\widehat{z}}\right| \\ &= \frac{\left|A_0 \mp \widehat{u}_0\right| + \sqrt{{A_1}^2 + {\widehat{Z}_0}^2 + 2A_1\widehat{Z}_0\cos\varphi}}{\widehat{Z}_0}\end{aligned} \tag{29}$$

The absolute acceleration transmissibility is just the ratio of the amplitude of the absolute acceleration of the mass to that

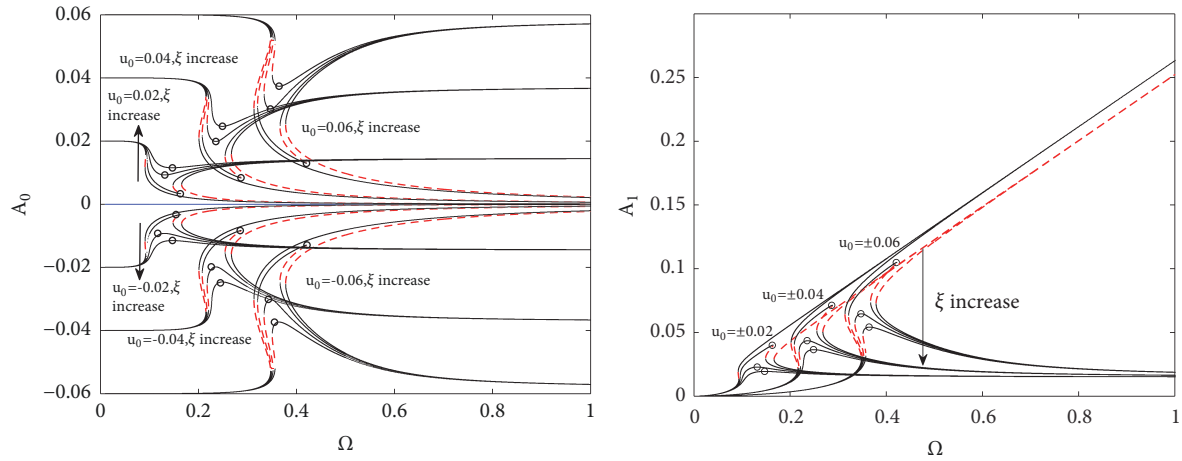

FIGURE 8: FRCs of overload and underload system with different offset displacements and damping ratio for the displacement excitation.

of the base and does not include the effect of the constant term. Its expression can be derived as

$$T_{\text{accel}} = \left|\frac{\widehat{u}''}{\widehat{z}''}\right| = \frac{\left|\widehat{v}'' + \widehat{z}''\right|}{\left|\widehat{z}''\right|} = \frac{\sqrt{A_1{}^2 + \widehat{Z}_0{}^2 + 2A_1\widehat{Z}_0\cos\varphi}}{\widehat{Z}_0} \tag{30}$$

For the ideal system, the absolute displacement and acceleration transmissibility have the same expression:

$$T_{\text{ideal}} = T_A = \frac{\sqrt{A_1{}^2 + \widehat{Z}_0{}^2 + 2A_1\widehat{Z}_0\cos\varphi}}{\widehat{Z}_0}, \tag{31}$$

where $\cos\varphi$ in (29), (30), and (31) can be determined in (20b) and setting $A_0 = 0$ in (29) for the ideal system.

Comparing (29) and (30), the difference is the bias term A_0. In (30), the effect of the bias term is eliminated. According to an investigation by Ravindra and Mallik [29], the absolute displacement transmissibility cannot perform satisfactorily with the isolation performance of a nonlinear isolator at high frequencies for the displacement excitation. Thus, in this paper, the absolute acceleration transmissibility is also considered to evaluate the isolation performance of the overload and underload systems more comprehensively.

The absolute displacement and acceleration transmissibility of the equivalent linear system are also the same, and the expression can be found in [6]:

$$T = T_D = T_A = \sqrt{\frac{1 + (2\xi\Omega)^2}{(1-\Omega^2)^2 + (2\xi\Omega)^2}} \tag{32}$$

3.3.2. Effects of the Excitation Amplitude, Offset Displacement, and Damping Ratio on the Transmissibility. A system under configurative parameters of the optimal value discussed in Section 2.2 and the damping ratio $\xi = 0.03$ is considered to study the transmissibility characteristics. Assuming that the offset $\widehat{u}_0 = \pm 0.02, \pm 0.04, \pm 0.06$, the excitation amplitude $\widehat{Z}_0 = 0.001, 0.01, 0.015$, and the damping ratio $\xi = 0.03, 0.05, 0.07$, the transmissibility of the overload and underload systems is studied, and the relative curves are presented in Figures 9–11, respectively. The transmissibility of the equivalent linear system and the ideal system is also illustrated for comparison. Note that all the transmissibility results are plotted in dB, i.e., as $20\log_{10}T$.

In these figures, it can be seen that the absolute displacement and acceleration transmissibility of the nonlinear isolator are different from each other significantly at the same excitation level. The absolute displacement transmissibility is larger than the absolute acceleration transmissibility in the entire frequency range. This agrees well with the analysis of (29) and (30). The isolation performance of the ideal system and the overload (underload) system may be better or worse than that of the linear system in different frequency ranges for different excitation amplitudes. For the same excitation amplitude, at low frequency, the transmissibility in descending order is the ideal system, the overload (underload) system, and the equivalent linear system. When the frequency skips over the resonance frequency of the ideal system, the transmissibility of the ideal system starts to decrease, and so does that of the overload (underload) system as the frequency is larger than its resonance frequency. In the region around the resonance frequency of the linear system, the transmissibility descending is the overload (underload) system, the equivalent linear system, and the ideal system. At high frequency, the absolute acceleration transmissibility of the three systems approaches the same level, while the absolute displacement transmissibility of the overload (underload) system is larger than that of the ideal and equivalent linear systems caused by the constant term. It is different from the FRCs that for the same offset displacement the overload and underload systems have the same transmissibility.

As shown in Figure 9, unlike the linear system which is not related to the excitation level, the peak amplitude and the corresponding resonance frequency of the absolute displacement and acceleration transmissibility for the overload

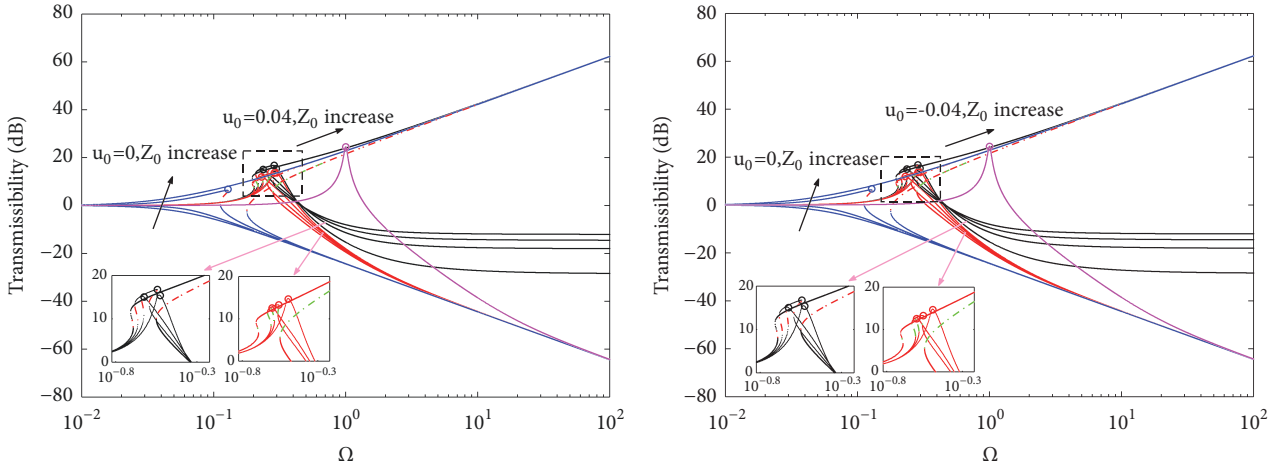

(a) For the overload system (b) For the underload system

FIGURE 9: Absolute displacement and acceleration transmissibility of the isolator and the equivalent linear system with different excitation amplitudes for the displacement excitation. "Red line": absolute displacement transmissibility. "Black line": absolute acceleration transmissibility. "Blue line": absolute displacement transmissibility of the ideal isolator. "Magenta line": the equivalent linear system. "Green and red dotted line": unstable solutions. "o": peak amplitude of transmissibility.

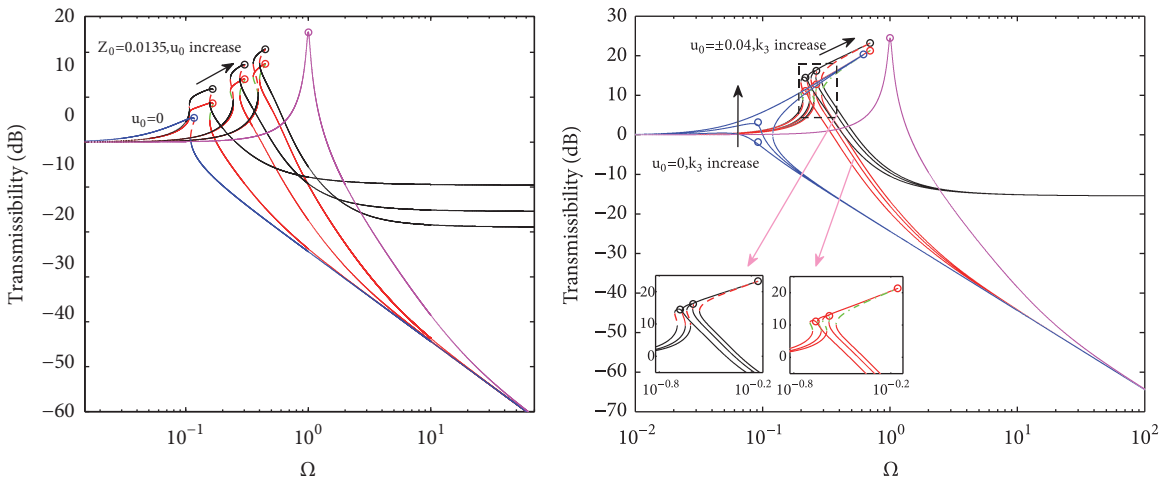

(a) For the offset displacement (b) For the cubic stiffness

FIGURE 10: Absolute displacement and acceleration transmissibility of the overload isolator and the linear system with different offset displacements and cubic stiffness (a) for the offset displacement and (b) for the cubic stiffness. "Red line": absolute displacement transmissibility. "Black line": absolute acceleration transmissibility. "Blue line": absolute displacement transmissibility of the ideal isolator. "Magenta line": the linear system. "Green and red dotted line": unstable solutions. "o" peak amplitude of transmissibility.

or underload system decrease first and increase later, and those of the ideal system increase as the excitation amplitude increases. The peak amplitude of the transmissibility may appear as an unbounded value when the excitation amplitude is large enough; it means the isolation performance becomes worse.

For a certain excitation amplitude, a smaller offset displacement results in a deviation toward the left of the transmissibility curve, a smaller peak amplitude, and a smaller resonance frequency. That is to say, the isolation frequency range of the system becomes wider, and the minimum isolation frequency tends to become lower, as the isolation performance increases. When the offset displacement disappears, the peak amplitude of the transmissibility and the corresponding resonance frequency have their minimum values, as shown in Figure 10. The cubic stiffness has the same effects on the transmissibility as well as the excitation amplitude. For the ideal isolator, larger cubic stiffness yields larger peak amplitude of the transmissibility. However, the peak amplitude of the absolute displacement and acceleration transmissibility for the overload (underload) system decreases at first, increases later, and may become unbounded as the cubic stiffness increases.

In Figure 11, for the ideal, overload (underload), and linear systems, when the damping ratio increases around

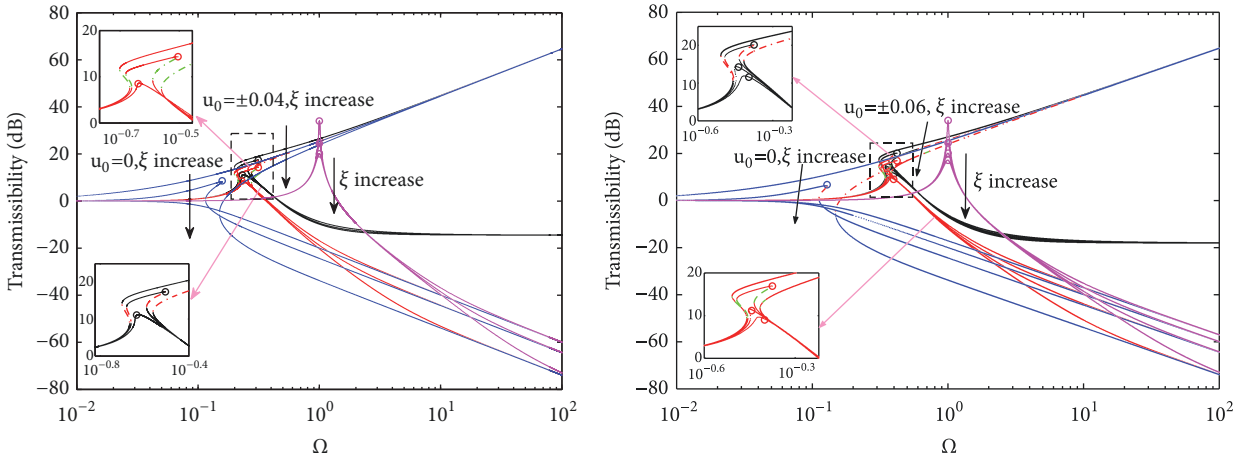

(a) $\widehat{u}_0 = \pm 0.04$ (b) $\widehat{u}_0 = \pm 0.06$

FIGURE 11: Absolute displacement and acceleration transmissibility of the overload isolator and the linear system with different damping ratios for the overload (underload) system. "Red line": absolute displacement transmissibility. "Black line": absolute acceleration transmissibility. "Blue line": absolute displacement transmissibility of the ideal isolator. "Magenta line": the linear system. "Green and red dotted line": unstable solutions. "o" peak amplitude of transmissibility.

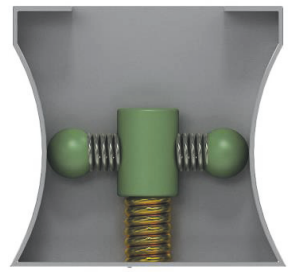

FIGURE 12: The prototype of the proposed nonlinear isolator.

the resonance frequency, the peak amplitude of the transmissibility decreases, and the corresponding resonance frequency decreases first and increases later. However, the transmissibility in the high frequency region increases accordingly, which means the isolation performance at higher frequencies worsens. For the ideal and overload (underload) system, the larger the damping ratio, the fewer the number of jump points. This means that the damper can be used to avoid the occurrence of jumps for the nonlinear isolator. In addition, if the damping ratio is large enough, the peak amplitude of the transmissibility for the ideal system will not occur, which implies that the isolation can isolate the vibration across the entire frequency range.

4. Experimental Investigation

4.1. Experimental Setup. A prototype of the proposed nonlinear isolator is built in this section to verify the isolation performance of the proposed system, as shown in Figure 12. The performance will be evaluated in terms of the acceleration transmissibility and compared among the overloaded and underloaded isolator and its linear counterpart, which is set by removing the curved-mount-spring-roller mechanism from the nonlinear isolator. The experimental setup is presented in Figure 13. The nonlinear isolator is rigidly mounted on the platform of a vibration exciter (4). The controller (1) is used to control the excitation displacement of the vibration exciter; the data acquisition and analyzer system (DASP, 2) executes data acquisition from four sensors symmetrically mounted between the base and isolator in order to measure the transmitted vibration from the base, and analyzes it. Four acceleration sensors (6, 10) are installed on the exciter and the mass to collect the excitation and the response acceleration. Two pairs of pliers (9) are used to firmly tighten the isolator to the platform support. The parameters of the experimental prototype of the nonlinear isolator are $R = 30$ mm, $r = 10$ mm, and $u_h = 0$. There are two coil springs in the horizontal direction and the stiffness of each of them is 50 N/mm, and the stiffness of the vertical spring is 25 N/mm. The rated mass of the isolator is 25 kg, and the corresponding theoretical resonance frequency of the linear system is calculated to be 5.04 Hz. The loaded

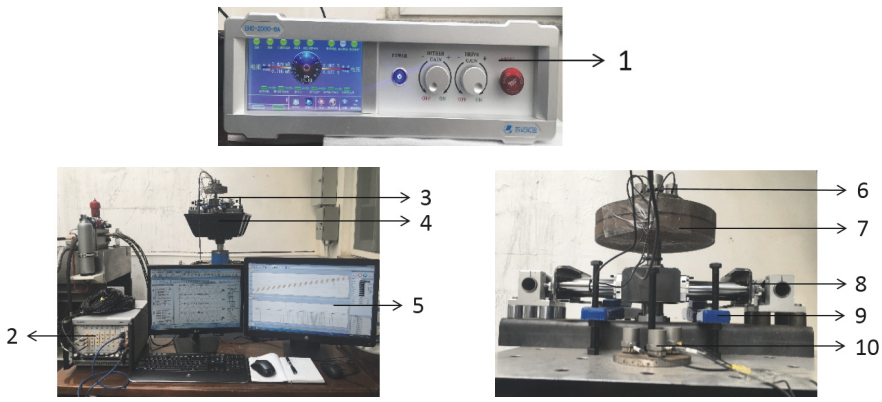

Figure 13: Experimental setup (1—controller for vibration exciter, 2—DASP, 3—the nonlinear isolation system, 4—exciter platform, 5—control screen for vibration exciter, 6—acceleration sensors acquiring the transmitted acceleration from the base, 7—mass, 8—the isolator, 9—pliers used to attach the system to the platform, 10—acceleration sensors acquiring the acceleration of the base).

mass is selected as 27.6 kg and 28.4 kg to realize overload and 22.5 kg to realize underload on purpose. The compression and offset displacements are listed in Table 2, which are calculated rather than measured. The nonlinear isolator system is rigidly fixed on the vibration exciter platform, and the maximum acceleration of the exciter platform is 4 g. For comparison, the nonlinear isolator, which is overloaded and underloaded at different levels, and its linear counterpart are subject to the performance test. In this experimental test, the base is subject to a sinusoidal displacement excitation from the hydraulic vibration table. The excitation frequency is from 0.2 Hz to 15 Hz, and the excitation amplitude is set from 3 mm to 5.5 mm. By using DASP, which is a data acquisition and analysis software package, the root-mean-square value for the displacements of the system response and the excitation can be obtained. The acceleration transmissibility is defined as the ratio of acceleration RMS (root-mean-square) value of the response and the excitation.

4.2. Experimental Results. The objective of this experiment is to compare the isolation performance of the overload (underload) system with the ideal system and the linear system. The experimental results of the acceleration transmissibility of the isolator which is overloaded and underloaded are shown in Figure 14 and compared with those of its linear counterpart and the ideal system. Vibration isolation plays a role when the transmissibility is lower than 1.

From the transmissibility in Figure 14, it can be seen that the performance of the nonlinear isolator is superior to the linear one in terms of the isolation frequency region. It is confirmed that the proposed curved-mount-spring-roller mechanism as a negative element can lower the dynamic stiffness of a linear isolator with positive stiffness. When the excitation amplitude increases, the peak transmissibility of the overload system and the corresponding resonance frequency decrease first and then increase, as shown in Figures 14(a) and 14(b). For the same offset and excitation amplitude, the transmissibility of the overload and underload systems is almost the same at the peak amplitude and the resonance frequency, and they are larger than that of the ideal system. This is indicated in Figure 14(c). It can be seen in Figure 14(d) that as the overload level increases, the offset displacement increases, and the peak transmissibility and the resonance frequency both become larger. However, the isolation performance of the overloaded system is still better than that of the linear system. All of these results agree well with the analysis conclusion above. However, for a large damping ratio, the jumping phenomenon did not appear, and there was no unbounded response because the response displacement was limited by rigid limiters.

Table 2: Parameters of the experimental prototype of the nonlinear isolation system.

Mass	Compression value	Offset value
28.4 kg	0.0111 m	0.00133 m
27.6 kg	0.0108 m	0.001 m
25 kg	0.0098 m	0 m
22.5 kg	0.0088 m	0.001 m

5. Conclusion

A nonlinear isolator composed of a curved-mount-spring-roller mechanism as the negative stiffness element and a vertical spring is studied theoretically and experimentally. The condition for achieving the zero stiffness at the static equilibrium position is obtained. Combinations of the configurative parameters are optimized for a wide displacement range around the static equilibrium position with a low dynamic stiffness and with the stiffness changing slightly.

The overload and underload conditions, which result in an offset displacement of the static equilibrium position from the zero-stiffness position, are taken into consideration. The differential equation of the motion is set up and the approximate solution is obtained by employing the HBM. The frequency response curves of the overload and underload system for the displacement excitation have been plotted with different parameters such as the excitation amplitude, the offset displacement, the damping ratio, and the cubic stiffness.

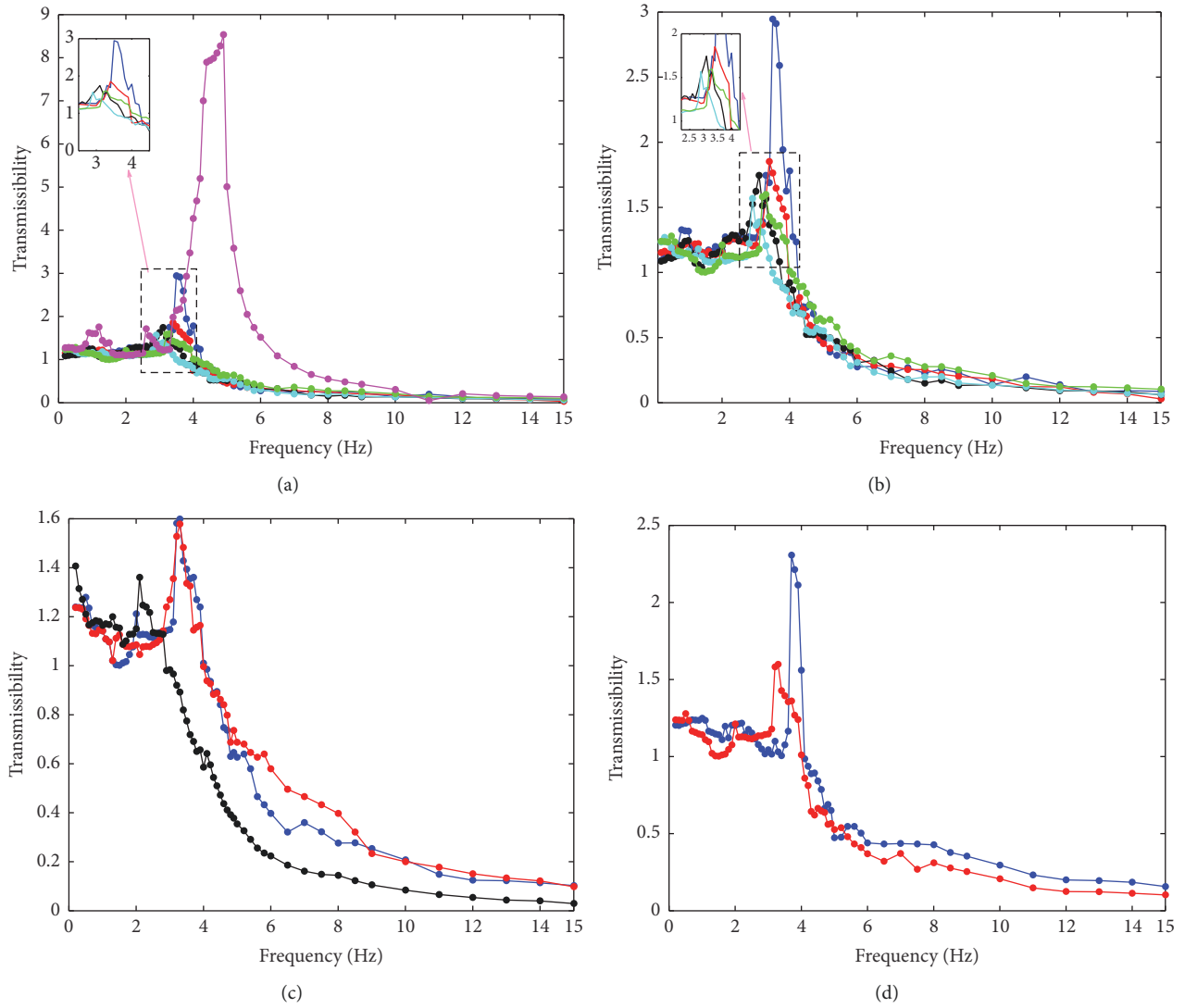

FIGURE 14: Experimental results for the acceleration transmissibility of the nonlinear and the linear isolator under different excitation amplitudes and the offsets: (a) overload system for excitation amplitude of 3 mm--green, 3.5 mm--cyan, 4 mm--black, 4.5 mm--red, 5 mm--blue, the linear system--magenta; (b) underload system for excitation amplitude of 3 mm--green, 3.5 mm--cyan, 4 mm--black, 4.5 mm--red, 5 mm--blue; (c) comparison among the ideal system--black, overload system--blue and underload system--red; and (d) overload system for the mass of 27.6 kg--red, 28.4 kg--blue.

According to the theoretical simulation, the system has the nonlinear behavior, and it has the linear, softening, softening-hardening, and purely hardening stiffness characteristics depending on the magnitude of the excitation amplitude and the excitation frequency. An unbounded response may occur as the excitation amplitude increases. Two kinds of transmissibility (the absolute displacement and acceleration transmissibility) are defined, and the isolation performance of the nonlinear isolator is evaluated by them. The transmissibility of the underload system is the same as that of the overload system; the transmissibility has nothing to do with the offset direction but its magnitude. Reducing the offset displacement and the excitation amplitude is helpful to improve the isolation performance of the isolator. Increasing the damping ratio is a way to decrease the peak amplitude of the response, avoid the jump phenomenon, and reduce the unstable region, but with the isolation performance for high frequency worsening.

Some experiments are carried out to validate the theoretical analysis. It is confirmed that, with the increase of the excitation amplitude, the acceleration transmissibility and the corresponding resonance frequency of the overload system decrease first and increase later. In addition, smaller offset displacement results in a smaller peak amplitude of the transmissibility and corresponding resonance frequency. The jump phenomenon did not appear in the experiment, probably because the damping ratio is too large.

Compared with the linear isolator, the nonlinear isolator has excellent low-frequency isolation performance whether under overload or underload state. The isolator with a negative stiffness element exhibits a better vibration isolation

performance when the excitation amplitude is not too large. For a certain nonlinear isolator, limiting the excitation amplitude and increasing the damper appropriately are effective ways to obtain better isolation performance. For a nonlinear isolator, appropriate overloaded or underloaded employing is beneficial to obtain a lower isolation frequency but a larger peak amplitude.

Nomenclature

a: Half of the curved-mount chord length
A: Amplitude of the linear system steady-state response
A_0: Constant term for the steady-state solution
A_1: Amplitude of harmonic term of the steady-state solution
A_{1p}: Peak amplitude of harmonic term of the ideal system
A_{0p}^o: Peak amplitude of the overload system
A_{0p}^u: Peak amplitude of the underload system
c: Damping coefficient
d: Displacement from the static equilibrium position
F: Restoring force of the QZS isolator
g: Acceleration of gravity
h: Initial height of the roller
k: Stiffness of the QZS isolator
k_0: Constant term of asymmetric excitation
k_3: Cubic stiffness coefficient in dynamic equation
k_h: Stiffness of the horizontal spring
k_v: Stiffness of the vertical linear spring
m: Weight of the mass
m_0: The rated mass weight
n: Integer
r: The radius of the roller
R: The radius of the curved mount
T: Transmissibility of the equivalent linear system
T_{disp}: Absolute displacement transmissibility
T_{accel}: Absolute acceleration transmissibility
T_{ideal}: Transmissibility of the ideal system
u: Relative displacement between the base and the isolated mass
u_0: Offset displacement
u_h: Initial compression length of horizontal springs
u_v: Initial compression length of the vertical spring
v: Transformed displacement of the mass under asymmetric excitation
x: Deflection of the vertical spring from the initial position
z: Displacement excitation
Z: Amplitude of the displacement excitation
α: Ratio of r to R
β: Ratio of a to R
λ: Stiffness ratio of k_h to k_v
ξ: Damping ratio
τ: Nondimensional time
ω: Excitation frequency
ω_n: Natural frequency of the isolator without negative stiffness mechanism
Ω: Frequency ratio ω/ω_n
Ω_p: Frequency corresponding to A_{1p}
Ω_{0p}^o: Frequency corresponding to A_{0p}^o
Ω_{0p}^u: Frequency corresponding to A_{0p}^u
φ: Phase of the response

Superscripts

$\dot{}$: Time derivative
$\hat{}$: Nondimensional quantity
$'$: Nondimensional time derivative.

Data Availability

All experimental data can be obtained on request from hanjunshu@163.com.

Conflicts of Interest

The authors declare that there are no conflicts of interest regarding the publication of this paper.

Acknowledgments

The research was supported by the National Science and Technology Major Project of China (NSTMPS) under Grant no. 2012ZX10004801-002-013.

References

[1] E. I. Rivin, *Passive Vibration Isolation*, ASME Press, New York, NY, USA, 2003.

[2] C. M. Harris and A. G. Piersol, *Shock and Vibration Handbook*, McGraw-Hill, New York, NY, USA, 2002.

[3] A. H. Nayfeh and D. T. Mook, *Nonlinear Oscillations*, John Wiley & Sons, New York, NY, USA, 1979.

[4] D. J. Mead, *Passive Vibration Control*, John Wiley and Son, 1999.

[5] A. Carrella, *Passive Vibration Isolators with High Static Low Dynamic Stiffness*, University of Southampton, 2008.

[6] L. N. Virgin and R. B. Davis, "Vibration isolation using buckled struts," *Journal of Sound and Vibration*, vol. 260, no. 5, pp. 965–973, 2003.

[7] J. Z. Zhang, D. Li, S. Dong, and M. J. Chen, "An ultra-low frequency parallel connection nonlinear isolator for precision instruments," *Key Engineering Materials*, vol. 257-258, pp. 231–236, 2004.

[8] W. G. Molyneux, "Ministry of Supply," Technical Note No. Structures 211, Supports for Vibration Isolation, UK, 1956.

[9] R. A. Ibrahim, "Recent advances in nonlinear passive vibration isolators," *Journal of Sound and Vibration*, vol. 314, no. 3–5, pp. 371–452, 2008.

[10] A. Carrella, M. J. Brennan, and T. P. Waters, "Static analysis of a passive vibration isolator with quasi-zero-stiffness characteristic," *Journal of Sound and Vibration*, vol. 301, no. 3–5, pp. 678–689, 2007.

[11] A. Carrella, M. J. Brennan, T. P. Waters, and V. Lopes Jr., "Force and displacement transmissibility of a nonlinear isolator with high-static-low-dynamic-stiffness," *International Journal of Mechanical Sciences*, vol. 55, no. 1, pp. 22–29, 2012.

[12] I. Kovacic, M. J. Brennan, and T. P. Waters, "A study of a nonlinear vibration isolator with a quasi-zero stiffness characteristic," *Journal of Sound and Vibration*, vol. 315, no. 3, pp. 700–711, 2008.

[13] I. Kovacic, M. J. Brennan, and B. Lineton, "Effect of a static force on the dynamic behaviour of a harmonically excited quasi-zero stiffness system," *Journal of Sound and Vibration*, vol. 325, no. 4-5, pp. 870–883, 2009.

[14] T. D. Le and K. K. Ahn, "A vibration isolation system in low frequency excitation region using negative stiffness structure for vehicle seat," *Journal of Sound and Vibration*, vol. 330, no. 26, pp. 6311–6335, 2011.

[15] L. D. Thanh and K. A. Kyoung, "Experimental investigation of a vibration isolation system using negative stiffness structure," *Mechanical Sciences*, vol. 158, pp. 1011–1029, 2013.

[16] P. M. Alabuzhev, A. A. Gritchin, P. T. Stepanov, and V. F. Khon, "Some results of an investigation of a vibration protection system with stiffness correction," *Soviet Mining Science*, vol. 13, no. 3, pp. 338–341, 1977.

[17] P. A labuzhev, A. Gritchin, L. Kim et al., *Vibration Protecting and Measuring Systems with Quasi-Zero Stiffness*, Hemisphere Publishing, New York, NY, USA, 1989.

[18] D. L. Platus, "Negative-stiffness-mechanism vibration isolation systems," in *Proceedings of the Vibration Control in Microelectronics, Optics, and Metrology*, vol. 1619, pp. 44–54, International Society for Optics and Photonics, San Jose, CA, USA, 1991.

[19] D. L. Platus, "Negative-stiffness-mechanism vibration isolation systems," in *Proceedings of the Optomechanical Engineering and Vibration Control*, Proceedings of the SPIE, pp. 98–105, July 1999.

[20] J. Yang, Y. P. Xiong, and J. T. Xing, "Dynamics and power flow behaviour of a nonlinear vibration isolation system with a negative stiffness mechanism," *Journal of Sound and Vibration*, vol. 332, no. 1, pp. 167–183, 2013.

[21] H. Guangjun, Z. Shengtong, and L. Hongguang, "Static analysis and experiment of a nonlinear vibration isolator," *Journal of Noise and Vibration Control*, vol. 31, no. 6, pp. 69–71, 2011.

[22] X. T. Liu, X. C. Huang, and H. X. Hua, "On the characteristics of a quasi-zero stiffness isolator using Euler buckled beam as negative stiffness corrector," *Journal of Sound and Vibration*, vol. 332, no. 14, pp. 3359–3376, 2013.

[23] X.-T. Liu, J.-Y. Sun, F. Xiao, and H.-X. Hua, "Principle and performance of a quasi-zero stiffness isolator for micro-vibration isolation," *Journal of Vibration and Shock*, vol. 32, no. 21, pp. 69–73, 2013.

[24] X. Huang, X. Liu, H. Hua et al., "Vibration isolation characteristics of a nonlinear isolator using Euler buckled beam as negative stiffness corrector: A theoretical and experimental study," *Journal of Sound and Vibration*, vol. 212, pp. 2319–2336, 2014.

[25] Y. Zhenhua, *Study on the Static and Dynamic Characteristics of Nonlinear Seat for Off-road Vehicles*, JiLin University, Changchun, China, 2014.

[26] M. Lingshuai, *Design and Characteristics Analysis of the Novel Quasi-zero Stiffness Isolator*, Academy of Military Medical Science, Beijing, China, 2015.

[27] R. Xudong, *Characteristics Analysis and Application Study of the Quasi-zero Stiffness Isolator Using Air Spring*, Academy of Military Medical Science, Beijing, China, 2017.

[28] C. Yushu, *Nonlinear Vibrations (in Chinese)*, Higher Education Press, Beijing, China, 2002.

[29] B. Ravindra and A. K. Mallik, "Performance of non-linear vibration isolators under harmonic excitation," *Journal of Sound and Vibration*, vol. 170, no. 3, pp. 325–337, 1994.